



CHORUS

This is the accepted manuscript made available via CHORUS. The article has been published as:

From Phase to Microphase Separation in Flocking Models: The Essential Role of Nonequilibrium Fluctuations

Alexandre P. Solon, Hugues Chaté, and Julien Tailleur

Phys. Rev. Lett. **114**, 068101 — Published 12 February 2015

DOI: [10.1103/PhysRevLett.114.068101](https://doi.org/10.1103/PhysRevLett.114.068101)

From Phase to Micro-Phase Separation in Flocking Models: The Essential Role of Non-Equilibrium Fluctuations

Alexandre P. Solon,¹ Hugues Chaté,^{2,3,4} and Julien Tailleur¹

¹Université Paris Diderot, Sorbonne Paris Cité, MSC, UMR 7057 CNRS, 75205 Paris, France

²Service de Physique de l'État Condensé, CNRS URA 2464, CEA-Saclay, 91191 Gif-sur-Yvette, France

³LPTMC, CNRS UMR 7600, Université Pierre & Marie Curie, 75252 Paris, France

⁴Beijing Computational Science Research Center,

3 Heqing Road, Haidian District, Beijing 100080, China

We show that the flocking transition in the Vicsek model is best understood as a liquid-gas transition, rather than an order-disorder one. The full phase-separation observed in flocking models with Z_2 rotational symmetry is however replaced by a micro-phase separation leading to a smectic arrangement of traveling ordered bands. Remarkably, continuous deterministic descriptions do not account for this difference, which is only recovered at the fluctuating hydrodynamics level. Scalar and vectorial order parameter indeed produce different types of number fluctuations, which we show to be essential in selecting the inhomogeneous patterns. This highlights an unexpected role of fluctuations in the selection of flock shapes.

Many of the phenomena heretofore only invoked to illustrate the many facets of active matter are now being investigated in careful experiments, and more and more sophisticated models are built to account for them. For flocking alone, by which we designate the collective motion of active agents, spectacular results have been obtained on both biological systems [1–9] and man-made self-propelled particles [10–12]. Nevertheless, it is fair to say that the current excitement about flocking takes place while our understanding of the simplest situations remains unsatisfactory. This is true even for idealized self-propelled particles interacting only via local alignment rules, as epitomized by the Vicsek model (VM) [13] which stands out for its minimality and popularity. Twenty years after the introduction of this seminal model for the flocking transition, and despite the subsequent extensive literature [14], we still lack a global understanding of the transition to collective motion.

It took a decade to show that the transition to collective motion in the VM, initially thought to be critical [13], was discontinuous [15]: upon increasing the density or reducing the noise strength, high-density bands of spontaneously aligned particles form suddenly [15] (Fig 1). The homogeneous ordered “Toner-Tu” phase [16] is only observed after a second transition at significantly lower noise/higher density [15]. Since then, hydrodynamic-level deterministic descriptions have been established and shown to support band-like solutions [17–19], but it was recently proved [20] that many such different solutions generically coexist. In fact, the connection of these results to microscopic models remains elusive. More generally, we lack a unifying framework encompassing the two transitions (disorder-bands, bands-Toner-Tu phase).

Such a global picture was recently proposed for the active Ising model (AIM), where rotational invariance is replaced by a discrete symmetry [22]: particles carrying Ising spins diffuse in space with a constant-amplitude bias along one arbitrarily fixed direction $\pm \mathbf{u}_x$, the sign

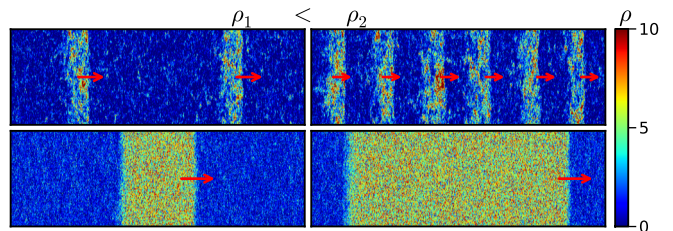


FIG. 1. Top: Micro-phase separation in the Vicsek model. $\eta = 0.4$, $v_0 = 0.5$, $\rho_1 = 1.05$ (left), $\rho_2 = 1.93$ (right). Bottom: Phase separation in the Active Ising model. $D = 1$, $\varepsilon = 0.9$, $\beta = 1.9$, $\rho_1 = 2.35$ (left), $\rho_2 = 4.7$ (right). System sizes 800×100 . Red arrows indicate the direction of motion.

being given by the local magnetization (see [31] for a detailed definition). The emergence of flocking in this model is akin to a liquid-gas transition between an ordered liquid and a disordered gas. Unlike the traveling bands of the VM, inhomogeneous profiles in the AIM are fully phase-separated, with a single macroscopic liquid domain traveling in the gas (Fig 1). More generally, the symmetry difference between the two models questions the relevance of this framework for the VM.

In this Letter, we show that the flocking transition in the Vicsek model is also best understood in terms of a liquid-gas transition—rather than an order-disorder one—but with *micro phase* separation in the coexistence region. Contrary to what was previously believed, we indeed show that the dense ordered bands discovered in [15] for the VM are arranged *periodically* in space, leading to an effectively “smectic” phase. We define an appropriate “liquid fraction” which allows us to recover the linear scaling across the coexistence region of a liquid-gas transition, hence closing a long-standing debate on the nature of the transition in the VM. But our most important results concern the hydrodynamic descriptions of flocking models. Surprisingly, deterministic hydrodynamic equations for scalar (AIM) and vectorial (VM) order param-

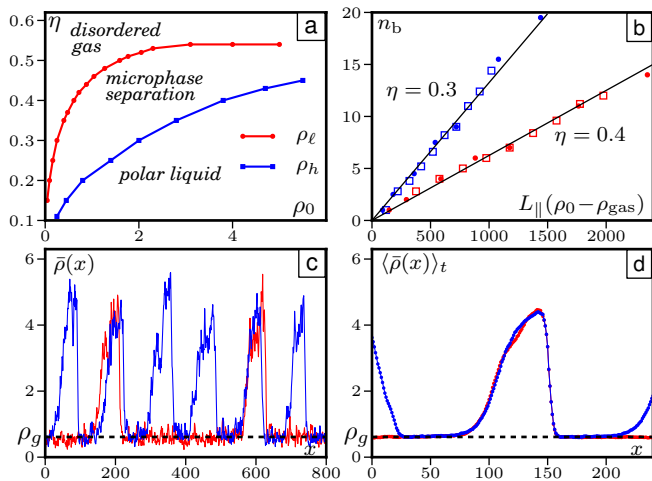


FIG. 2. **a**: Phase diagram of the Vicsek model. The binodals $\rho_\ell(\eta)$ and $\rho_h(\eta)$ mark the limit of the coexistence region. **b**: Number of bands vs $L_{\parallel}(\rho_0 - \rho_{\text{gas}})$ varying either the excess density for $Lx \times Ly = 2000 \times 100$ (squares) or the system size along the direction of propagation (dots) for $\rho_0 = 0.6$ ($\eta = 0.3$) or $\rho_0 = 1.2$ ($\eta = 0.4$). The straight black lines are guide for the eyes. **c**: Density profiles of Fig. 1 averaged along the transverse direction \mathbf{e}_{\perp} , $\bar{\rho}(x_{\parallel}) = \langle \rho(x_{\perp}, x_{\parallel}) \rangle_{x_{\perp}}$. **d**: Time average of the band profiles shown in **c**. A three-fold increase of the excess density changes the number of bands but not the gas density or the shape of the bands. $v = 0.5$, $\eta = 0.4$, $\rho_0 = 1.05$ (red), $\rho_0 = 1.93$ (green).

ter *both* support many different coexisting *stable* inhomogeneous solutions selected by initial conditions, including single-domain and micro-phase smectics. They thus do not account for the differences observed in the microscopic models. We then show that the two scenarios are however discriminated at the *fluctuating* hydrodynamic level: the different symmetries result in qualitatively different density fluctuations, effectively providing a selection criterion. Scalar and vectorial stochastic partial differential equations indeed generically lead to different, unique profiles, in agreement with the microscopic models.

We first recall the definition of the Vicsek model. N point-like particles, labeled by index i , move at constant speed v_0 on a rectangular plane of surface $S = L_x L_y$ with periodic boundary conditions. At each discrete time step $\Delta t = 1$, the headings θ_i of all particles are updated in parallel according to [28]

$$\theta_i(t+1) = \langle \theta_j(t) \rangle_{j \in \mathcal{N}_i} + \eta \xi_i^t \quad (1)$$

where \mathcal{N}_i is the disk of unit radius around particle i , ξ_i^t a random angle drawn uniformly in $[-\pi, \pi]$, and η sets the noise intensity. Then, particles hop along their new headings: $\mathbf{r}_i(t+1) = \mathbf{r}_i(t) + v_0 \mathbf{e}_i^{t+1}$, where \mathbf{e}_i^{t+1} is the unit vector pointing in direction given by $\theta_i(t+1)$.

In agreement with [15], we find, varying the noise η and the density $\rho_0 = N/S$, three different phases: a dis-

ordered gas at high noise/low density, a polar liquid at low noise/high density, and an intermediate region where ordered bands travel in a disordered background. In the thermodynamic limit, the homogeneous phases are separated from the coexistence phase by two “binodals”: $\rho_\ell(\eta)$, $\rho_h(\eta)$, which are reported on Fig 2-a. One could in principle add spinodal lines in the coexistence region, marking the limits of linear stability of the homogeneous phases. At finite “temperature” η , nucleation prevents us from computing them directly but quenching the system into the coexistence region, we see two distinct behaviors: metastability and nucleation close to the coexistence lines, spinodal decomposition deeper in the coexistence region (see movies in [31]). As for the AIM, an important difference with the phase diagram of a liquid-gas phase transition in the canonical ensemble is its unusual shape, which stems from the different symmetries of the two phases. Since it is impossible to go continuously from the polar liquid to the disordered gas, there is no supercritical region and the critical point is sent to $\rho_c = \infty$.

While the phase diagrams of VM and AIM have similar shapes, their coexistence regions are fundamentally different. Starting from random initial conditions, the dynamics of the VM rapidly leads to randomly spaced ordered bands propagating along a direction \mathbf{e}_{\parallel} and spanning the system along \mathbf{e}_{\perp} , as reported before [15, 17]. On much longer time-scales, *unreached in previous studies*, the relaxation of compression modes actually leads to *regularly* spaced bands (See Fig. 2-c and movie in [31]). In the thermodynamic limit, the bands have well-defined profiles, *independent from the average density and the system size*. In this limit, increasing ρ_0 at constant η thus does not change the density ρ_{gas} of the gaseous background, nor the celerity or the shape of the bands. Only the band number n_b increases, proportionally to $L_{\parallel}(\rho_0 - \rho_{\text{gas}})$ (Fig. 2-b&d). For finite systems, the quantization of the liquid fraction has some interesting consequences. An excess mass $S(\rho_0 - \rho_{\text{gas}})$ which is not a multiple of the excess mass m_b of a single band does not allow the system to relax to its asymptotic band-shape. To accommodate this excess mass the bands are slightly deformed, but c and ρ_{gas} barely change as ρ_0 is varied (not shown).

This smectic arrangement of finite-width bands markedly differs from the more conventional liquid-gas phase-separation seen in the AIM, where increasing the density simply widens the single liquid domain. One may thus wonder whether all features of the liquid-gas scenario survive. The global polarisation $|\mathbf{P}| = \frac{1}{N} |\sum_i \mathbf{e}_i|$, used in previous studies of the VM to characterize the onset of ordering [13, 15, 17], does not show a linear increase of the liquid fraction with density (Fig 3-a). Such a scaling is however recovered by considering $|\mathbf{v}| \equiv \frac{1}{S} |\sum_i v_0 \mathbf{e}_i| = v_0 \rho_0 |\mathbf{P}|$ (Fig 3-b). Indeed, for a propagating band of celerity c , integrating the continuity

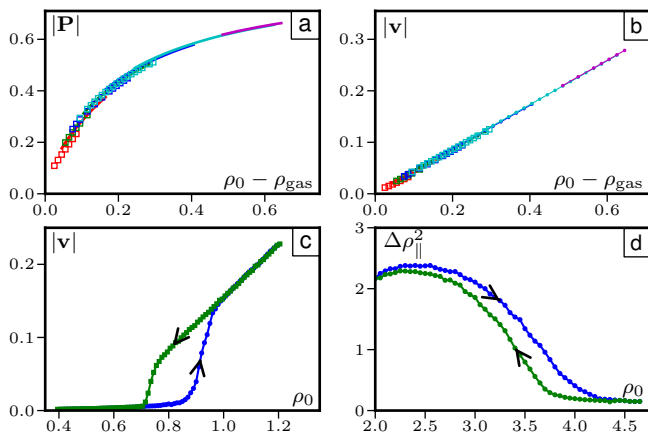


FIG. 3. Polarisation (a) and mean velocity (b) vs ρ_0 for $L=2048$ (squares) and $L=1024$ (lines). Red, green, blue, cyan and magenta correspond to 1-5 band solutions. c: Hysteresis loop between gas and micro-phase states. d: Hysteresis loop between micro-phase and liquid states. The variance $\Delta\rho_{\parallel}^2$ quantifies inhomogeneity along the direction of motion. 100 runs are used for c and d, with $\eta = 0.4$, system size 400×400 .

equation $\dot{\rho} = -\nabla \cdot \mathbf{W}$, where $\mathbf{W}(\mathbf{r}) = \sum_i \delta(\mathbf{r} - \mathbf{r}_i) v_0 \mathbf{e}_i$ is the momentum field, yields $c(\rho(\mathbf{r}) - \rho_{\text{gas}}) = W_{\parallel}(\mathbf{r})$ [17]. Averaging over space, this gives $|\mathbf{v}| = c(\rho_0 - \rho_{\text{gas}})$. Since c and ρ_{gas} barely depend on ρ_0 , $|\mathbf{v}|$ scales linearly with $\rho_0 - \rho_{\text{gas}}$, even for finite systems where nearby values of n_b coexist (See Fig 3-b). This is yet another signature of the first-order nature of the transition and confirms the analogy with the canonical liquid-gas transition; the apparent singularity of $|\mathbf{P}|$ close to ρ_{gas} is a simple consequence of its normalisation, not of criticality (as often assumed in the literature).

Close to $\rho_{\ell}(\eta)$, we observe expected hysteresis loops [15] when ramping ρ_0 up and down, with two sharp jumps in the mean velocity $|\mathbf{v}|$ (Fig. 3-c). Their interpretation is now much clearer: if the ramping is slow enough, they correspond to the nucleation and vanishing of a single band which acts as a critical nucleus. Indeed, a band can only be observed if the excess density $\rho_0 - \rho_{\text{gas}}$ is of the order of m_b/S . As the system size increases, bands are hence seen closer and closer to ρ_{gas} which thus coincide with the binodal ρ_{ℓ} , as in a standard liquid-gas transition. Moreover, the critical nucleus contains a smaller and smaller fraction of the particles as L increases so that $|\mathbf{v}|$ and $|\mathbf{P}|$ vary *continuously* to zero in the infinite-size limit (cf. Fig 3-a,b), something which had been missed before.

The second transition line $\rho_{\ell}(\eta)$ between the smectic micro-phase and the ordered liquid is harder to locate accurately. For $\rho_0 \lesssim \rho_h(\eta)$, the bands are indeed closely packed and interact strongly. Although global orientational order remains high, they break and merge in a chaotic manner (See movie in [31]). The resulting dynamics is thus difficult to distinguish from the giant density

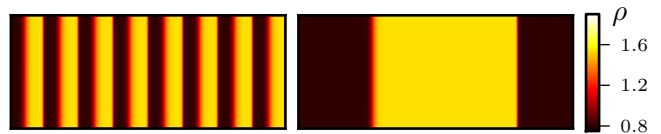


FIG. 4. Density field in the PDEs after integration over $t = 10^5$. **Left**: scalar PDE, ordered initial condition with a periodic perturbation. **Right**: vectorial PDE, disordered initial condition. Parameters: $\lambda = \rho_c = D = P_0 = 1$, $\rho_0 = 1.2$. System size 800×100 .

fluctuations of the homogeneous phase. Following [15], we use $\Delta\rho_{\parallel}^2 \equiv \langle (\bar{\rho}(x_{\parallel}) - \rho_0)^2 \rangle_{x_{\parallel}}$, the variance along L_{\parallel} of $\bar{\rho}$, the density profile averaged in the transverse direction. Fig. 3-d shows that hysteresis loops also exist around the transition line $\rho_{\ell}(\eta)$, which we define as the high-density end-point of the loops. **This allows us to provide for the first time a complete phase diagram of the VM in Fig 2.**

To account for the differences between the coexistence phases of the VM and AIM, we now connect the above results to the more theoretical level of continuous descriptions. There are two important differences between the hydrodynamic equations of VM and AIM: the nature of the ordering field (vectorial in the VM, scalar in the AIM) and the functional dependencies of the transport coefficients on density and momentum fields. When looking for one-dimensional traveling solutions, the dimension of the ordering field however becomes irrelevant. Furthermore, it was recently shown [20] that hydrodynamic equations of flocking models admit such traveling solutions with both smectic micro-phases and phase-separated profiles. We have checked that both types of solutions exist for both the equation proposed for the AIM [22] and for those proposed for Vicsek-like models [17].

Since [20] only established the existence of these solutions, a possibility to account for the different inhomogeneous profiles seen in VM and AIM could be that these solutions have different *stability* in the corresponding two-dimensional equations, where the dimension of the order parameter can play a role. To test this hypothesis, we consider scalar and vectorial versions of the “same” minimal two-dimensional partial differential equations (PDE). The first one, sPDE, has a scalar magnetization field W corresponding to the AIM discrete symmetry

$$\begin{aligned} \partial_t \rho &= -\partial_x W \\ \partial_t W &= \left[(\rho - \rho_t) - \frac{W^2}{P_0^2 \rho} \right] W + \nu \nabla^2 W - \partial_x \rho - \lambda W \partial_x W \end{aligned} \quad (2)$$

The second set, vPDE, has a vectorial momentum \vec{W} in line with the continuous rotational symmetry of the VM

$$\begin{aligned} \partial_t \rho &= -\nabla \cdot \vec{W} \\ \partial_t \vec{W} &= \left[(\rho - \rho_t) - \frac{|\vec{W}|^2}{P_0^2 \rho} \right] \vec{W} + \nu \nabla^2 \vec{W} - \nabla \rho - \lambda (\vec{W} \cdot \nabla) \vec{W} \end{aligned} \quad (4)$$

$$\partial_t \vec{W} = \left[(\rho - \rho_t) - \frac{|\vec{W}|^2}{P_0^2 \rho} \right] \vec{W} + \nu \nabla^2 \vec{W} - \nabla \rho - \lambda (\vec{W} \cdot \nabla) \vec{W} \quad (5)$$

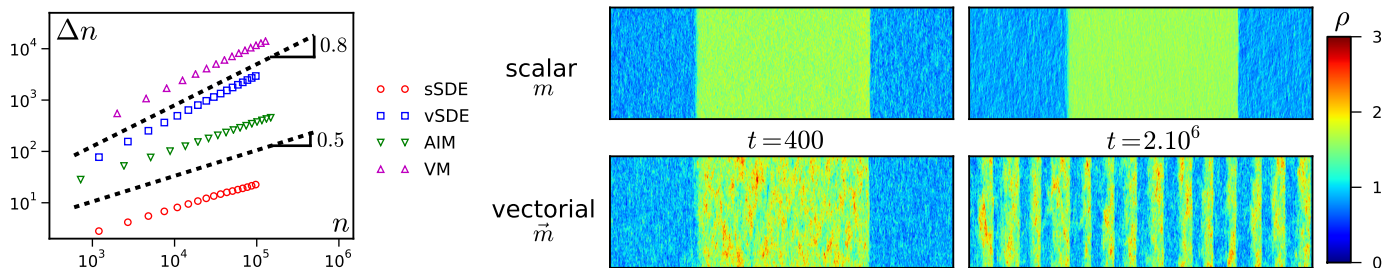


FIG. 5. **Left:** Number fluctuations $\Delta n = \sqrt{\langle n^2 \rangle - \langle n \rangle^2}$ where n is the number of particles in boxes of different sizes. Measures done in the homogeneous liquid phase. Parameters: size 400×400 (all), $\rho_0 = 5$, $\beta = 2.4$ (AIM), $\rho_0 = 5$, $\eta = 0.4$ (VM), $\lambda = \rho_c = D = P_0 = 1$, $\gamma^2 = 0.4$, $\rho_0 = 3$ (sSDE and vSDE). **Right:** Numerical integration of sSDE (top) and vSDE (bottom). Parameters: $\rho_c = \lambda = D = P_0 = 1$, $\gamma^2 = 0.4$, system size 2000×100 .

Clearly, the disordered solution $|W| = 0$ becomes linearly unstable for $\rho_0 > \rho_t$. As in all active matter systems with metric interactions, the homogeneous ordered solution $|W|^2 = \rho_0(\rho_0 - \rho_t)P_0^2$ that emerges from this mean-field transition is itself linearly unstable to long wavelengths until $\rho_0 > \rho_s$ [17, 18, 20]. Note that ρ_t and ρ_s correspond to the spinodal lines mentioned above. Most of the inhomogeneous solutions classified in [20] exist in a ρ_0 range wider than $[\rho_t, \rho_s]$. It is possible to estimate ρ_{\min} and ρ_{\max} , the extremal values of ρ_0 between which solutions exist. For instance, setting all parameters including ρ_t to unity as in Fig. 4, one finds $\rho_{\min} \simeq 0.808$, $\rho_s \simeq 1.25$, and $\rho_{\max} \simeq 1.74$.

We integrated numerically these two sets of equations for various parameter values inside and outside the $[\rho_t, \rho_s]$ interval [29]. After transients, we end up with effectively one-dimensional solutions taking constant values along \mathbf{e}_\perp . In all cases we found both smectic micro-phases and phase-separated profiles. Which solution is observed depends only on the initial condition and not on the symmetry of the ordering field. Fig. 4 shows a periodic solution in the sPDE and a single traveling domain in the vPDE obtained for the same parameter values, a striking evidence that the (deterministic) hydrodynamic equations alone *cannot* explain the selection of different patterns observed in microscopic models. This result was found robust to modifications of Eqs. (2)-(5).

We call sSDE and vSDE the stochastic versions of Eqs. (2-5) obtained by adding a zero-mean scalar (or vectorial) Gaussian white noise of variance $\gamma^2 \rho (1 - \frac{|W|^2}{\rho^2})$ in the W (or \vec{W}) equation [30]. Integrating first sSDE and vSDE in the homogeneous liquid phase, we recover the same density fluctuations as in the corresponding microscopic models (Fig. 5 left): normal fluctuations in sSDE, giant ones in vSDE (with the same scaling as in microscopic models). More importantly, we recover the correct type of inhomogeneous profiles in each case, irrespective of the initial conditions. For instance, starting from a large liquid domain as initial condition in both sets of equations with the same parameters, we find that sSDE keeps this configuration while it breaks down in vSDE,

eventually leading to a periodic array of bands (Fig. 5 right). In the converse experiment, starting from a configuration with many bands, we observe initially merging events in both cases but this process stops in vSDE, leading to an asymptotic periodic state with a finite number of bands, while coarsening proceeds for sSDE.

We conclude that fluctuations play an essential role in selecting the phase-separated patterns. Note that similar experiments performed in microscopic models yield similar results. For instance, in the VM at relatively high noise large liquid domains are metastable for a long enough time to be observed before fluctuations break them and lead the system to the smectic micro-phase state (see movie in [31]). Giant density fluctuations break large liquid domains and arrest band-coarsening while normal fluctuations do not. Two different scenarios emerge: In the active Ising class, magnetization is a scalar quantity, density fluctuations are normal and the system undergoes bulk phase separation. In the active XY or Vicsek class, magnetization is vectorial, density fluctuations in the liquid are anomalously large and drive the system to the micro-phase separated state.

To summarize, we have shown that the flocking transition in the Vicsek model amounts to a micro-phase liquid-gas transition in the canonical ensemble exhibiting metastability, hysteresis and coexistence between a disordered gas and a smectic arrangement of liquid bands. This is in contrast with the bulk phase separation exhibited by the active Ising model [22]. We found that while (deterministic) hydrodynamic equations do *not* explain this difference, their stochastic counterparts do: the different nature of the order parameter produces different types of number fluctuations, which are essential in selecting the phase-separated patterns. This unexpected role of fluctuations in the selection of flock shapes calls for a greater care when trying to account for active systems based on purely deterministic continuum equations.

Interesting questions remain open. For example, the mechanism by which the bands interact in the VM to reach a periodic spacing and the chaotic behavior of closely packed bands are still to be investigated. Fur-

ther, we so far have no analytical approach and limited numerical results to ascertain the stability of the smectic pattern in the direction along the bands. It is not inconceivable that, like recently found in active nematics [23], the coexistence phase is asymptotically disordered. Last, in the large density region, the finite sizes of real flocking agents are not negligible and steric effects such as motility-induced phase separation [24–26] could enrich the simple liquid-gas scenario [27].

We thank the Max Planck Institute for the Physics of Complex Systems, Dresden, Germany and the Kavli Institute for Theoretical Physics, Santa Barbara, USA, for hospitality. This research was supported in part by the National Science Foundation under Grant No. NSF PHY11-25915.

-
- [1] V. Schaller, C. Weber, C. Semmrich, E. Frey and A. R. Bausch, *Nature* **467**, 7377 (2010); V. Schaller and A. R. Bausch, *Proc. Natl. Acad. Sci. USA* **110** 4488-4493 (2013).
- [2] Y. Sumino, K. H. Nagai, Y. Shitaka, D. Tanaka, K. Yoshikawa, H. Chaté and K. Oiwa, *Nature* **483**, 448-452 (2012).
- [3] M. Ballerini, N. Cabibbo, R. Candelier, A. Cavagna, E. Cisbani, I. Giardina, V. Lecomte, A. Orlandi, G. Parisi, A. Procaccini, M. Viale, V. Zdravkovic, *Proc. Natl. Acad. Sci. USA* **105** 1232 (2008).
- [4] T. Sanchez, D. T. Chen, S. J. DeCamp, M. Heymann, Z. Dogic, *Nature* **491**, 431-434 (2012).
- [5] S. Zhou, A. Sokolov, O. D. Lavrentovich, I. S. Aranson, *Proc. Natl. Acad. Sci.* **111**, 1265-1270 (2012).
- [6] A. Sokolov, I. S. Aranson, J. O. Kessler and R. E. Goldstein *Phys. Rev. Lett.* **98** 158102 (2007).
- [7] F. Peruani, J. Starruss, V. Jakovljevic, L. Sogaard-Andersen, A. Deutsch, and M. Br, *Phys. Rev. Lett.* **108**, 098102 (2012)
- [8] Y. Katz, K. Tunstrøm, C. C. Ioannou, C. Huepe, I. D. Couzin, *Proc. Natl. Acad. Sci. USA* **108**, 18720-25 (2011).
- [9] J. Gautrais, F. Ginelli, R. Fournier, S. Blanco, M. Soria, H. Chaté, G. Theraulaz, *Plos Comp. Biol.* **8**, e1002678 (2012).
- [10] J. Deseigne, O. Dauchot, H. Chaté. *Phys. Rev. Lett.* **105**, 098001 (2010); J. Deseigne, S. Léonard, O. Dauchot, H. Chaté, *Soft Matt.* **8**5629-5639 (2012); C. A. Weber, T. Hanke, J. Deseigne, S. Léonard, O. Dauchot, E. Frey, H. Chaté, *Phys. Rev. Lett.* **110**, 208001 (2013).
- [11] S. Thutupalli *et al.*, *New J. Phys.* **13** 073021 (2011).
- [12] A. Bricard, J-B. Caussin, N. Desreumaux, O. Dauchot, D. Bartolo, *Nature* **503**, 9598 (2013).
- [13] T. Vicsek, A. Czirók, E. Ben-Jacob, I. Cohen, O. Shochet, *Phys. Rev. Lett.* **75**, 1226 (1995).
- [14] T. Vicsek, A. Zafeiris, *Phys. Rep.* **517**, 71 (2012).
- [15] G. Grégoire, H. Chaté, *Phys. Rev. Lett.* **92** 025702 (2004); H. Chaté, F. Ginelli, G. Grégoire, F. Raynaud, *Phys. Rev. E* **77** 046113 (2008).
- [16] J. Toner and Y. Tu, *Phys. Rev. Lett.* **75**, 4326 (1995); *Phys. Rev. E* **58**, 4828 (1998); J. Toner, *Phys. Rev. E* **86** 031918 (2012).
- [17] E. Bertin, M. Droz, G. Grégoire, *Phys. Rev. E* **74** 022101 (2006); *J. Phys. A* **42** 445001 (2009); A. Peshkov, E. Bertin, F. Ginelli and H. Chaté, *Eur. Phys. J Special Topics* **223**, 1315 (2014).
- [18] S. Mishra, A. Baskaran, M.C. Marchetti. *Phys. Rev. E* **81**, 061916. (2010); A. Gopinath, M.F. Hagan, M.C. Marchetti, A. Baskaran. *Phys. Rev. E* **85**, 061903. (2012)
- [19] T. Ihle, *Phys. Rev. E* **83**, 030901 (2011); T. Ihle, *Phys. Rev. E* **88**, 040303(R) (2013).
- [20] J.-B. Caussin, A. Solon, A. Peshkov, H. Chaté, T. Dauxois, J. Tailleur, V. Vitelli, and D. Bartolo, *Phys. Rev. Lett.* **112**, 148102 (2014)
- [21] N. Guttenberg, J. Toner, and Y. Tu, *Phys. Rev. E* **89**, 052711 (2014)
- [22] A.P. Solon, J. Tailleur, *Phys. Rev. Lett.* **111**, 078101 (2013).
- [23] S. Ngo, A. Peshkov, I.S. Aranson, E. Bertin, F. Ginelli, and H. Chaté, arXiv:1312.1076 (2013); X. Shi, H. Chaté and Y. Ma, *New J. Phys.* **16** 035003 (2014).
- [24] J. Tailleur, M. E. Cates, *Phys Rev Lett.* **100** 218103 (2008).
- [25] Y. Fily and M. C. Marchetti, *Phys. Rev. Lett.* **108**, 235702 (2012).
- [26] G. S. Redner, M. F. Hagan, and A. Baskaran, *Phys. Rev. Lett.* **110**, 055701 (2013)
- [27] F. D. C. Farrell, J. Tailleur, D. Marenduzzo, M. C. Marchetti, *Phys. Rev. Lett.* **108**, 248101 (2012).
- [28] This defines the angular noise dynamics of the Vicsek model. Vectorial noise dynamics do not introduce any qualitative difference [15].
- [29] For the PDEs and SDEs we used a pseudo-spectral integration scheme (linear terms are computed in Fourier space, non-linear ones in real space) using semi-implicit time-stepping. SDEs were integrated following Itô's interpretation.
- [30] This structure of the noise variance is one of the simplest that accounts for the observed fact that the amplitude of fluctuations decreases when polarization $|W|/\rho$ increases while respecting the symmetry of the ordering field. However, our results are not sensitive to this particular form and hold for simpler choices such as $\gamma^2\rho$ or even additive noise.
- [31] See Supplemental Material at XXX for movies and more information.